ELSEVIER

Surface and Coatings Technology 146–147 (2001) 175–182

SURFACE & COATINGS TECHNOLOGY

www.elsevier.com/locate/surfcoat

Mechanical properties of superhard nanocomposites

Stan Veprek[a,*], Ali S. Argon[b,1]

[a]*Institute for Chemistry of Inorganic Materials, Technical University Munich, Lichtenbergstrasse 4, D-85747 Garching b, Munich, Germany*
[b]*Department of Mechanical Engineering, Massachusetts Institute of Technology, 77 Massachusetts Avenue, Cambridge, MA 02139, USA*

Abstract

Novel superhard nanocomposites prepared according to the generic design concept [Thin Solid Films 268, (1995) 64], which is based on the formation of the appropriate nanostructure due to strong segregation and spinodal decomposition, show an unusual combination of mechanical properties, such as high intrinsic (i.e. not falsified by a large compressive stress) Vickers microhardness from 40 to $\geq$100 GPa, high elastic recovery (up to $\geq$90%), high resistance against crack formation even at a large strain of $\geq$10% and high thermal stability. We shall show that these properties can be relatively easily understood on the basis of conventional fracture mechanics scaled down to dimensions of a few nanometers small nanocrystals and nanocracks, in combination with a low concentration of possible flaws introduced into the material during its preparation. The latter is a consequence of the 'self-organization' of the system due to the thermodynamically driven formation of the stable nanostructure.

Keywords: Nanocomposites; Superhard; Nanostructure; Mechanical properties

1. Introduction

A variety of superhard nanocomposites made of nitrides, borides and carbides was prepared recently by several research groups using plasma-induced chemical and physical vapor deposition (CVD and PVD, respectively, and laser ablation; for a recent review see [2]). In the appropriately synthesized binary systems, the hardness of the nanocomposite exceeds significantly that given by the rule of mixtures in bulk. For example, the hardness of nc-M_nN/a–Si_3N_4 (M = Ti, W, V,…) nanocomposites with the optimum content of Si_3N_4 close to the percolation threshold reaches 50 GPa [1–9] although that of the individual nitrides does not exceed 21 GPa. Similar results were reported also for several other systems by other researchers (see [2]). In the case of a binary solid solution, such as $TiN_{1-x}C_x$, the hardness increases with increasing x monotonically from that of TiN to the hardness of TiC, thus following the rule of mixtures [5].

Recently, Musil et al. have achieved superhardness also in coatings consisting of a hard transition metal nitride and a soft metal which does not form thermodynamically stable nitrides, such as nc-M_nN–M′ (M = Ti, Cr, Zr, M′ = Cu, Ni; for a review see [10]). However, these systems have shown a low thermal stability and decrease of the hardness upon annealing to $\geq$400°C due to the relaxation of a high biaxial compressive stress built in the films during the deposition and possibly also due to a miscibility of the components [11,12].

The generic concept for the design of novel, superhard nanocomposites which are stable up to high temperatures of $\geq$1000°C, which is very important for their industrial applications, is based on thermodynamically driven segregation in binary (and ternary) systems which display immiscibility and undergo spinodal decomposition even at such temperatures [1,7,8]. The condition for spinodal decomposition in a binary system $A_{1-x}B_x$ to occur is a negative second derivative of the free energy of formation of the mixed phase $A_{1-x}B_x$ with an infinitesimal change of the composition $A_{1-x\pm\delta}B_{x\pm\delta}$,

* Corresponding author. Tel.: +49-89-2891-3624; fax: +49-89-2891-3626.
E-mail address: veprek@ch.tum.de (S. Veprek).
[1] argon@mit.edu

0257-8972/01/$ - see front matter
PII: S0257-8972(01)01467-0

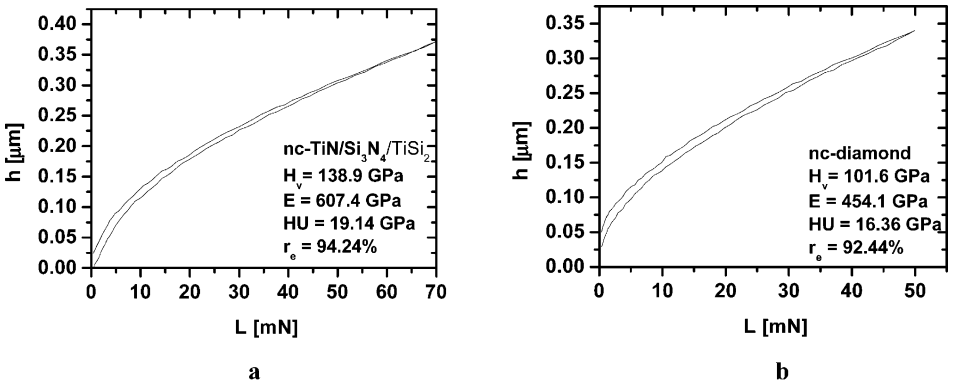

Fig. 1. Comparison of the indentation curves for ultrahard nanocomposites nc-TiN/a–Si_3N_4/a– and nc-$TiSi_2$ [25] (a) and the hardest diamond coating which we obtained from various laboratories (b). Notice that a lower applied load was used for the nc-diamond.

i.e. $d^2(\Delta G^0)/dx^2 < 0$ [13]. Therefore, any small local fluctuation of the composition of the mixed phase decreases the free energy of the system thus leading to a spontaneous segregation. As a result, a nanocomposite forms which remains stable against coarsening (Ostwald ripening) as long as the condition $d^2(\Delta G^0)/dx^2 < 0$ remains valid [13–15].

In this paper we shall concentrate on such systems that remain stable at a high temperature, retain their superhardness and that were sufficiently characterized in terms of the nanostructure, the composition of the phases, thermal stability and mechanical properties. In particular, we do not consider here coatings where the measured enhancement of the apparent hardness and elastic modulus were due to a high biaxial compressive stress (see [2,16,17] and references therein). The latter is commonly observed in PVD deposited films where the compressive stress is typically 4–6 GPa and can even exceed values of 10 GPa. For example, Herr and Broszeit [18] reported a hardness of 72 GPa for HfB_2 coatings sputter-deposited at a low pressure of 5×10^{-3} mbar which introduced a high biaxial compressive stress of approximately 7 GPa. Upon annealing at 650°C the stress and the hardness decreased to 2 and 17 GPa, respectively. Musil et al. [19] reported hardness of 100 GPa for (TiAlV)N films deposited by sputtering at low pressure and having also a high biaxial compressive stress. These authors did not perform any annealing experiments in order to verify what the real, 'intrinsic' hardness of their films was. Nevertheless, the hardness of TiN coatings of approximately 80 GPa reported in the same paper and of 70 GPa reported by the same author in a later publication [20] suggests that these measured values were falsified by the high compressive stress induced by energetic ion bombardment. However, more recent results indeed support this view [11,12]. In order to exclude the possible artefacts due to (in the majority of papers unknown) high compressive stress in the films, we shall use here only those results where either a low residual stress of <1 GPa was measured and reported or the hardness did not change after annealing up to the recrystallization temperature of 800–1100°C [7–9].

2. The meaning of hardness and elastic modulus in superhard nanocomposites as measured by means of indentation

The measurement of the hardness of thin hard coatings by means of indentation can be subject to a number of errors ([2,21] and references therein), particularly when, due to a small thickness of the films, small loads have to be used which may cause an apparent increase of the measured hardness (so called 'indentation size effect') as found e.g. for ceramics [22] and diamond [23] and explained in terms of a finite distance between the deformation bands [22]. Therefore, our reported data are based on: the load independent values (typically between 50 and 200 mN where the indentation depth does not exceed 10% of the film thickness of typically 4–20 μ); absence of creep [2,24]; and comparison with Vickers hardness evaluated from the size of the remaining plastic deformation measured in scanning electron microscope (SEM) [25]. Because the superhard nanocomposites show a very high elastic recovery from 80 [1,6] to $>90\%$ [25] (see also Fig. 1) it is important to compare the whole indentation curves with those of well defined materials, such as diamond, as shown in Fig. 1.

One sees that the shape of the loading and unloading curves are very similar, as are also the high value of the 'universal hardness' HU (the hardness under load, see inserts in Fig. 1a,b) which underlines the high strength of the nanocomposites. Although the shapes of the unloading curves, from which the elastic modulus is evaluated, suggest a predominantly elastic behavior, it is important to check if the nature of the indentation meets the criterion of elastic indentation response according to classical Hertzian indentation solution [26].

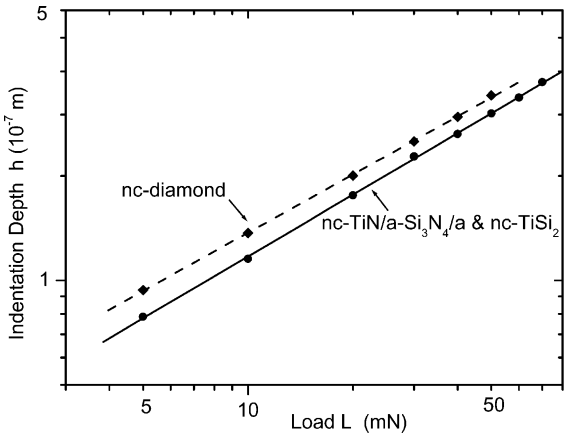

Fig. 2. The 'Hertzian' plot of the indentation depth h vs. applied load L.

In first approximation, this can be assessed by means of the Hertzian elastic response under a spherical indenter of radius R and contact circle radius a, assuming for simplicity the same elastic moduli of the indenter and the coating because of the close agreement of these values (see Fig. 1). The analysis of the Hertzian indentation into an elastic, semi-infinitive material gives a dependence of the indentation depth $h(L)$ on the applied load L (for details see Timoshenko and Goodier [26]):

$$\ln h(L) = \frac{1}{3}\left[-\ln\left(\frac{E^2 \cdot R}{1.861}\right)\right] + \frac{2}{3}\ln L \qquad (1)$$

Fig. 2 shows the log–log dependence of the indentation depth on the applied load for the nc-TiN/a–Si_3N_4/a– and nc-$TiSi_2$ ($E = 607$ GPa) and nc-diamond ($E = 454$ GPa) coatings which corresponds to the indentation curves in Fig. 1. One sees a very good log–log straight line behavior with slopes 0.585 and 0.6 for the nc-diamond and nc-TiN/a–Si_3N_4/a– and nc-$TiSi_2$, respectively. The relatively small difference from the true Hertzian slope for ideally elastic materials of $2/3 = 0.667$ is due to the fact that the indentations are not purely elastic and that the indenter geometry of the Vickers diamond is not exactly spherical. Taking the plot of Fig. 2 and the elastic moduli of the materials of the coatings, the radius of the tip of the indentor can be calculated from Eq. (2):

$$h = 1.23\left(\frac{L^2}{E^2 \cdot R}\right)^{\frac{1}{3}} \qquad (2)$$

giving values of $R = 0.448$ and 0.385 μm for nc-diamond and nc-TiN/a–Si_3N_4/a– and nc-$TiSi_2$ coatings which are in a reasonably good agreement with each other and with that of the Vickers diamond indenter [27].

This analysis shows clearly that the major portion of the h vs. L response as measured by the indentation into the super- and ultrahard nanocomposite coatings is a simple Hertzian elastic indentation. Furthermore, the high values of the elastic moduli and of the universal hardness HU (hardness under the maximum applied load, Fig. 1) underline the fact that these materials are indeed very strong, and that the observed extraordinary high 'plastic hardness' is not due to any 'rubber-like' elastic response. Because rubber is not plastic, its hardness cannot be related to a flow stress in terms of the 'plastic hardness' but rather to its elastic stiffness, which would show as a very small universal hardness and elastic modulus.

Beside of the elastic deformation there is also an irreversible plastic deformation observed in the superhard nanocomposites whose energy corresponds to the area between the loading and unloading curves and which can be measured in micrographs taken after the indentation (see [8,25] and below). Because the lack of dislocation activity in 3–5-nm small nanocrystals, their strength approaches the ideal value. Thus, the plastic deformation must come from localized shear events within the intercrystalline 'amorphous' component. Only if of percolative nature, such shear events will result in localization in the form of shear bands as reported by

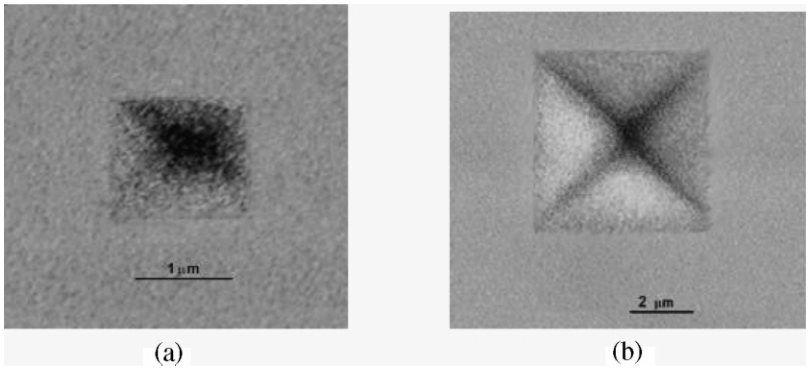

Fig. 3. Examples of the appearance of the remaining indentation into: (a) 3.5-μm thick ultrahard coating from Fig. 1a after applied load of 100 mN, (b) 10.7-μm thick superhard coating ($H_{0.01} \approx 40$ GPa) with a load of 1000 mN.

various researchers (e.g. [22]). However, because no such deformation bands were observed in our nanocomposites in a large number of SEM micrographs even after an indentation at a very high load (Fig. 3b), we conclude that the individual shear events have remained spatially isolated. Furthermore, the existence of a load independent value of the measured plastic hardness, together with the absence of deformation bands and with the high thermal stability, lend a strong support to the conclusion that the value of plastic hardness obtained from the indentation measurement and checked by the evaluation of the size of the remaining plastic deformation do represent the correct properties of these materials.

Another possible mechanism contributing to the plastic deformation is densification of the material due to the high pressure under the indenter (see below). Future investigations by means of high resolution transmission electron microscopy may help to answer the question which of these possible mechanisms is dominant.

3. The origin of the enhancement of the measured elastic modulus

It is generally accepted that hardness of bulk materials scales with the value of shear modulus because the plastic deformation of crystalline materials is due to dislocation activity and the energy of a dislocation is proportional to the shear modulus [28,29]. Therefore, it was not surprising to find a similar correlation between the indentation hardness H and the elastic modulus measured by the indentation technique (E_{ind}) in the superhard nanocomposites [1,6]. The ratio of H^3/E_{ind}^2 was discussed as an important criterion of the resistance against plastic deformation for hard materials by Tsui et al. [30] and emphasized as an important criterion of mechanical properties for superhard nanocomposites by Musil [10]. However, the very high values of the composite elastic modulus as found for superhard nanocomposites which are in the range of diamond or even higher (see e.g. Fig. 1a above and Fig. 1 in Musil [10]) pose the question regarding their physical meaning. Let us therefore consider which fundamental properties of a material determine its elastic constants.

The bulk modulus B is given by the second derivative of the crystal energy U_{c} with dilatation [31]:

$$B = -\left(\frac{d(V/V_0)}{dP}\right)^{-1} = V_{\mathrm{mole}}^2 \frac{\delta^2 U_C}{\delta V^2} \tag{3}$$

In other terms, the bulk modulus is a measure of the increase of the crystal energy with a change of the volume imposed by an external hydrostatic pressure as given by the third term in Eq. (4):

$$U_{\mathrm{C}}(V) = U_{\mathrm{C}}(V_0) + \left(\frac{\delta U_{\mathrm{C}}}{\delta V}\right)_{V_0} \cdot \delta V + \frac{1}{2}\left(\frac{\delta^2 U_{\mathrm{C}}}{\delta V^2}\right)_{V_0} \cdot \delta V^2 + \ldots \tag{4}$$

Here V_0 is the molar volume at zero pressure and $U_{\mathrm{C}}(V_0)$ is the crystal energy at equilibrium, i.e. $(\delta U_{\mathrm{C}}/\delta V)_{V_0} = 0$. Thus, the increase of the crystal energy upon hydrostatic pressure is given by the increase of the curvature of the potential surface in three dimensions. In a similar way, Young's modulus E_y can be approximated by the second derivative of the binding energy with bond distance and related to the shear modulus by the equation $G = E_y/2(1+\nu)$ where ν is the Poisson's ratio [32]. These relations have a simple physical meaning: the higher the interatomic binding energy and coordination number and smaller the bond distance, the higher the elastic moduli. Carbon in its diamond polymorph meets best the condition of the combination of a high covalent interatomic bond energy, the highest coordination number for covalent bond and a small interatomic distance. Therefore, it has the highest values of elastic moduli. Unlike the strength and hardness, which are limited by flaws in materials (dislocations and microcracks) and therefore orders of magnitude smaller than the ideal values, elastic moduli are determined by the atomic structure. For these reasons, values of elastic modulus of the superhard nanocomposites in the range of diamond or even higher, as measured by an indentation technique, are suspected to be an artefact of that technique.

The 'effective' elastic modulus E_{eff} is calculated from the slope S of the unloading portion of the indentation curve as [21,27,32] (here β is a constant given by the indenter geometry and A is the contact area between the indenter and the material to be measured, elastic modulus E_{i}, Poisson's ratio ν_{i})

$$E_{\mathrm{eff}} = \frac{S \cdot \sqrt{\pi}}{2\beta\sqrt{A}} \tag{5}$$

and corrected for the elastic deformation of the indenter

$$\frac{1}{E_{eff}} = \frac{1-\nu^2}{E} + \frac{1-\nu_{\mathrm{i}}^2}{E_{\mathrm{i}}} \tag{6}$$

in order to obtain the elastic modulus of the material E. Based on Sneddon's solution for the indentation of an elastic half-space by a rigid axisymmetric indenter [33], the latter is usually associated with the Young's modulus [21,27]. However, Sneddon's solution appeared to be somewhat inaccurate [34,35] and for superhard materials further effects should be accounted for. One of them is the so far unknown mechanism of the deformation of the material and of the indenter, which means that the measured modulus E_{ind} is likely to be a more complex combination of the elastic constants. The other, more illustrative effect is the very high pressure under the

indenter present during the measurement on such materials. Let us consider this problem in some detail.

As already pointed out by Tabor [36] the indentation hardness H is a direct measure of the average pressure P under the indenter,

$$H(\text{GPa}) \cong \text{const.} \cdot P(\text{GPa}) \quad (7)$$

where the constant accounts for the difference between the projected area of the indentation and the exact area of the contact between the indenter and the material (for Vickers indenter it is equal to 0.927). Under conditions of yielding (i.e. plastic deformation) of the material under the indenter, the yield pressure is essentially constant and independent of the applied load:

$$P = \frac{H}{\text{const.}} = \frac{L}{A} \quad (8)$$

where A is the area of the remaining indentation. The higher the hardness the smaller the area A and the higher the average pressure under the indenter, i.e.

$$P(L = \text{const..}) \propto H_{\text{plast}} \quad (9)$$

Of course, the distribution of the stress under the indenter is complex. It was calculated only for several simple cases [36,37]. Nevertheless, for a given, constant applied load L the pressure under the indenter increases with increasing hardness as seen from Eq. (8) and Eq. (9) and can reach very high values of the order of 40–60 GPa for superhard nanocomposites.

An example par excellence of high compressive stress upon the indentation process is the semiconductor-to-metal transition in silicon which commences at approximately 11.3 and is completed at 12.5 GPa. This transition is observed upon indentation with a Vickers indenter at an applied load of approximately 30–40 mN and it is best seen on the unloading curve.[2] It is accompanied by a strong decrease of electric resistivity of silicon within the indentation area (see [38] and references therein). Gridneva et al. reported the semiconductor-to-metal transition upon indentation in Si, Ge, InSb and GaAs and has shown that the pressure under the indenter at which this transition occurs determines the measured hardness of the given material [39].

Fig. 4 shows the elastic moduli of a number of nc-TiN/a–Si_3N_4/a– and nc-$TiSi_2$ nanocomposites measured by indentation and corrected for the elastic deformation of the diamond indenter. The samples differed only by the total content of silicon (between 0 and approx. 20 at.%), different fractions of the amorphous a–Si_3N_4 and amorphous and nanocrystalline

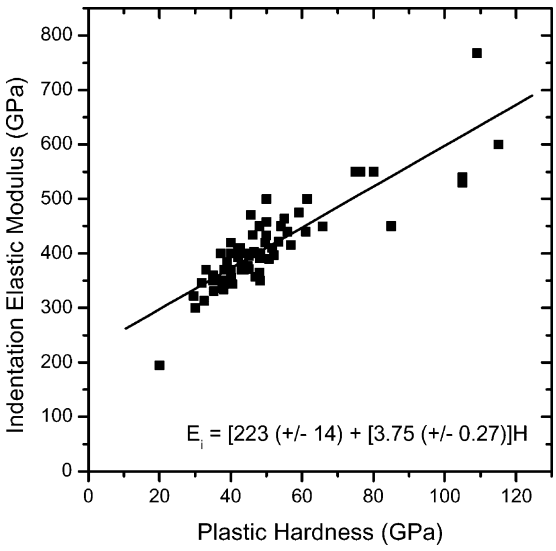

Fig. 4. Elastic modulus of nc-TiN/a–Si_3N_4/a– and nc-$TiSi_2$ nanocomposites measured by indentation and corrected for the deformation of the diamond indenter vs. the plastic hardness.

$TiSi_2$ and different crystallite size, the main component being TiN [25]. In spite of that, the elastic indentation modulus varied by almost a factor of 4 showing a proportionality $E_{\text{ind}} \approx (3.75 \pm 0.27)\ H$. Our earlier published binary superhard nanocomposites nc-TiN/a–Si_3N_4, nc-W_2N/a–Si_3N_4 and nc-VN/a–Si_3N_4 have shown also a linear increase of the elastic modulus with the plastic hardness having somewhat larger proportionality factors [1,5,6]. Musil summarized similar data for several other superhard nanocomposite coatings prepared by reactive sputtering and obtained a proportionality factor of approximately 5 (Fig. 1 in [10][3]). Thus, the experimental data available so far for a fairly large number of different superhard nanocomposites show an approximately linear increase of the elastic modulus with the plastic hardness as measured by the indentation, the proportionality factor being between approximately 3.7 and 9.

Let us now consider the dependence of elastic moduli on pressure. The increase of bulk modulus with pressure, $\partial B/\partial P$ is due to the increase of the crystal energy with decreasing distances between the atoms, i.e. due to the increasing curvature of the interatomic potential surface. That increase depends on the nature of binding and of the crystal lattice, but the values of the first derivative of B with P, $\partial B/\partial P$, are within a relatively small range

[2] This transition appears as a 'noise' on the loading curve and as a sudden jump of the unloading curve to a lower indentation depth when a maximum load used for the Vickers indenter does not exceed 100 mN. However, if a larger load of $\geq$150 mN is used, a similar jump is found upon unloading at approximately 120–140 mN due to cracking and peeling of the material.

[3] Although — as mentioned above — in some of these coatings prepared by plasma PVD the apparent plastic hardness is most probably enhanced by the high compressive biaxial stress the correlation between the measured elastic modulus E_{ind} and the values of that hardness still represents the effect of the pressure under the indenter because Eqs. (7) and (8) remain valid.

of approximately 3–8 for the majority of materials, as summarized below.

Grover et al. [40] have shown that under compression, the logarithm of the isothermal bulk modulus of many metals increases almost linearly with the decrease of the specific volume $-\Delta V/V_0$ up to volume changes of 40%. The slope of these dependencies varied for different metals within the range of approximately 3–8 in agreement with theoretical calculations [41,42] and many later experimental data (e.g. [43,44]). Rose et al. [45] derived a universal zero-temperature equation of state which allowed them to calculated the first derivative of bulk modulus as a universal function of the ratio of the Wigner–Seitz atomic radius at equilibrium, r_{WSE}, to the width of the interatomic binding energy curve l, which corresponds to the anharmonicity of the crystal.

$$\left(\frac{\partial B}{\partial P}\right)_T = 1 + \frac{2.3}{3}\frac{r_{WSE}}{l} \tag{10}$$

This expression yields theoretical values in a fairly good agreement with the experimental ones for a large number of solids (see Table III in [45]). In a more recent paper these authors extended their consideration also to the interfaces [46]. Thus, the pressure dependence of elastic moduli can be fairly well approximated by proportionality:

$$B(P) = B_0 + A \cdot P \tag{11}$$

with B_0 being the bulk modulus at zero pressure and A is a constant for a given material with a value between approximately 3 and 8. Similar pressure dependences of Young's and shear moduli is a consequence of their mutual relationships via the Poisson's ratio [32].

The close quantitative similarity between the measured proportionality for the indentation elastic modulus E_{ind} found for superhard nanocomposites (see above) and in Eqs. (7)–(9) and Eq. (11) strongly supports the idea that the high values of E_{ind} measured for the superhard nanocomposites under a very high pressure of many 10 GPa are due to the pressure enhancement and, thus, an artefact of that technique. Because such a pressure enhancement is relatively small for softer materials it is not surprising that their E_{ind} values agree within the accuracy of the measurements with those measured by other techniques [47]. Independent measurements of the elastic moduli of superhard nanocomposites by means of other techniques and detailed finite element modeling of the indentation process are highly desirable.

4. The high elastic recovery, energy of the elastic deformation and resistance against crack formation

The energy of elastic deformation as measured in the indentation experiment can be estimated from the area between the unloading curve and the y-axes in Fig. 1

$$U_{el} = \int_0^{h_{max}} L(h) \cdot dh \tag{12}$$

to be approximately 1×10^{-8} J. Similar values can be estimated also from a number of other indentations on such coatings. Assuming the total area of the deformation under the maximum applied load of 0.07 N (Fig. 1a) to be approximately four times the area of the permanent, plastic deformation as obtained from the load-depth sensing indentation measurements and SEM micrographs (see Fig. 3a), we estimate the elastic energy density of approximately 3×10^8 J m^{-3}, and finally the specific elastic energy of approximately 3 kJ mole^{-1}.

Let us compare this value with the elastic energy U_{el} of an ordinary solid, in its linear range, as given by Eq. (13).

$$U_{el.} = V_{mole} \cdot \frac{B}{2} \cdot \left(\frac{\Delta V}{V}\right)_{el}^2 \tag{13}$$

[Here, B is the bulk modulus (of approx. $\leq$500 GPa) and $(\Delta V/V)_{el}$ is the true elastic dilatation.] Assuming as an upper limit for the elastic dilatation of 1% (i.e. much higher than what is typically found for hard materials) and $V_{mole} \approx 10$ cm^3 (10^{-5} m^3), the elastic energy density of the order of 0.5 kJ/mole results which is much smaller than the elastic energy density estimated from the indentation in the superhard materials. Let us briefly discuss the possible reasons for this discrepancy.

The possibility, that the elastic deformation extends to a much larger volume is unlikely because one would have to assume a total lateral area of a uniform elastic deformation to be approximately 24 times larger than that of plastic deformation. This is just the opposite as generally found because the elastic strain decreases very strongly with the distance from the center of the contact between the indenter and the material (see also the SEM micrographs in Fig. 3).

More likely, the nanostructured superhard nanocomposites can indeed sustain a much larger strain than the conventional hard materials for the following reasons: In the nanostructured materials with 3–5-nm size eqiaxed nanocrystals, the extension of the possible initial flaws induced by the high applied stress are at the scale of $\leq$1 nm, i.e. at a scale comparable with interatomic bond distance. It is well known that the rupture strain of interatomic bond can reach up to 20%. Moreover, the stress concentration factor [32] of such small nanocracks of approximately 2–4 remains very small thus preventing their catastrophic growth [9].

Thus, the high elastic energy density can be explained by a mechanism called 'reversible non-linear flexing' which is shown schematically in Fig. 5. The first derivative of the binding energy with bond distance (Fig. 5a) is the 'restoring force' which develops upon elastic deformation of interatomic bonds. The part of

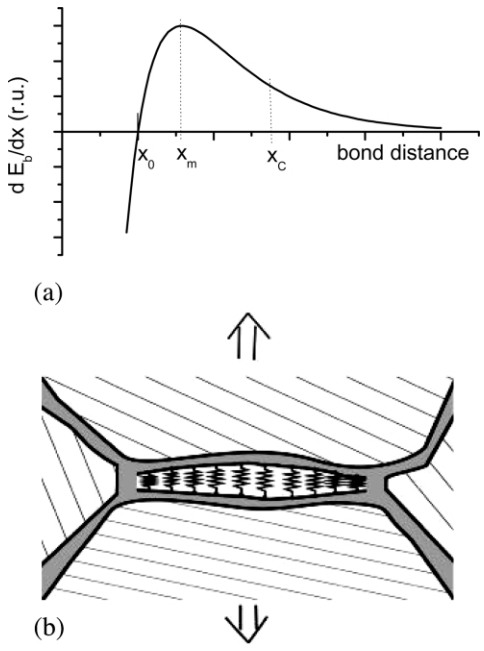

Fig. 5. (a) First derivative of the binding energy with bond distance; x_0 is the equilibrium bond distance. (b) Flexing of the bonds across the interface between the nanocrystals (see text).

that curve for bond distance $x \geq x_0$ is called the 'fundamental decohesion curve'. A single isolated bond would break when, under a constant applied stress when the dilatation associated with x exceeds x_m. However, if the cohesion of the nanostructure is provided by the attached nanocrystals, a much larger local strain in the interfaces in the flexing of $x_0 < x < x_m$ will be reversible because the restoring force $dE_b/dx > 0$ (Fig. 5a) and the interaction between the atoms persists (Fig. 5b). The elastic energy of the flexing with a dilatation corresponding to x_C is the area under the curve between x_0 and x_C. If the elastic strain energy associated with the elastic deformation of the attached nanocrystals remains less than the energy of flexing of the bonds across the interface, the system will continue to be stable and reversible and the energy of flexing of the entire system will fully recover upon unloading. Because the energy density of flexing per unit of the flexed volume will now be very high as compared with that of linear elastic deformation of conventional materials [Eq. (12)], flexing within a relatively small fraction of interfaces is sufficient to explain the high elastic energy associated with the high elastic recovery (for a more quantitative estimate see Veprek and Argon [15]).

The observed high resistance of the superhard nanocomposites against crack formation can be also understood in terms of conventional fracture mechanics scaled down to dimensions of 1–2 nm. As already mentioned, the stress concentration factor based on nanoscale flaws is low and, therefore, the stress needed to propagate such a small nanocrack is very high. Moreover, the propagation of such nanocracks in the three dimensional nanocomposites involves much deflection and branching of the plane of the cracks which again hinder the growth of the nanocracks. Last but not least, the self-organization of the system due to the thermodynamically driven spinodal segregation results in a very low concentration of built-in flaws. Thus, the remarkably high resistance of these nanocomposites against crack formation is easily understood in the terms of a high threshold for the initiation of larger microcracks which may lead to their catastrophic growth [25]. One does not need to evoke any enhancement of fracture toughness as defined by the stress intensity factor or energy release rate [32] for which there is no rational physical justification.

5. Conclusions

An analysis of the indentation curves measured on superhard nanocomposites in terms of Hertzian elastic response shows that they are indeed strong materials. The unusual combination of high plastic hardness with high elastic recovery and high resistance against crack formation and growth can be understood on the basis of conventional fracture mechanics scaled down to dimensions of a few nanometer sized nanocrystals and nanocracks, in a combination with a low concentration of possible flaws introduced into the material during its preparation. The latter is a consequence of the 'self-organization' of the system due to the thermodynamically driven formation of the stable nanostructure by the spinodal decomposition, and it provides these systems also the observed surprisingly high thermal stability.

The observed high resistance of such coatings against crack formation upon the indentation is a consequence of a very low concentration of critical flaws as a result of the self-organization of the nanostructure. It is unnecessary to evoke any enhancement of the fracture toughness in terms of stress intensity factor or energy release rate for which a physical basis was lacking.

The strong enhancement of the elastic modulus E_{ind} measured for the superhard nanocomposites by means of the indentation technique is most probably due to a very high pressure under the indenter. The measured correlation of E_{ind} with H_{plast} for a variety of superhard coatings supports this suggestion.

Extreme care should be exercised when measuring superhardness in thin coatings. In particular it is necessary to check if the apparent 'superhardness' is an intrinsic property of that material and not falsified by a high biaxial compressive stress or a too low load used for the measurements. Such coatings will loose their superhardness when annealed to a temperature of 500–600°C (or even less) [11,12].

Because of the limited available space we could not develop all the ideas here in sufficiently quantitative

detail. These details will be provided in the forthcoming full-length paper [15].

Acknowledgements

We should like to thank to the coworkers at TU Munich for fruitful collaboration with the sample preparation and characterization. This work has been supported in part by the German Science Foundation (DFG) and the NATO Science for Peace Program SfP 972379.

References

[1] S. Veprek, S. Reiprich, Thin Solid Films 268 (1995) 64.
[2] S. Veprek, J. Vac. Sci. Technol. A 17 (1999) 2401.
[3] L. Shizhi, S. Yulong, P. Hongrui, Plasma Chem. Plasma Process. 12 (1992) 287.
[4] S. Veprek, S. Reiprich, L. Shizhi, Appl. Phys. Lett. 66 (1995) 2640.
[5] S. Veprek, M. Haussmann, S. Reiprich, L. Shizhi, J. Dian, Surf. Coat. Technol. 86–87 (1996) 394.
[6] S. Veprek, M. Haussmann, S. Reiprich, J. Vac. Sci. Technol. A 14 (1996) 46.
[7] S. Veprek, P. Nesladek, A. Niederhofer, F. Glatz, M. Jilek, M. Sima, Surf. Coat. Technol. 108/109 (1998) 138–147.
[8] A. Niederhofer, P. Nesladek, H.-D. Männling, K. Moto, S. Veprek, M. Jilek, Surf. Coat. Technol. 120–121 (1999) 173.
[9] S. Veprek, A. Niederhofer, K. Moto et al., Surf. Coat. Technol. 133 (2000) 152.
[10] J. Musil, Surf. Coat. Technol. 125 (2000) 322.
[11] P. Karvankova, H.-D. Männling, Ch. Eggs, F.N. Regent, J. Musil, S. Veprek, Surf. Coat. Technol. (2002) submitted.
[12] P. Karvankova, H.-D. Männling, Ch. Eggs, S. Veprek, Surf. Coat. Technol. 146–147 (2001) 280.
[13] H. Schmalzried, Chemical Kinetics of Solids, VCH Verlag, Weinheim, 1995.
[14] H.-D. Männling, D.S. Patil, K. Moto, M. Jilek, S. Veprek, Surf. Coat. Technol. 146–147 (2001) 263.
[15] S. Veprek, A.S. Argon, J. Vac. Sci. Technol., submitted for publication.
[16] T.Y. Tsui, W.C. Oliver, G.M. Pharr, J. Mater. Res. 11 (1996) 752.
[17] A. Bolshakov, W.C. Oliver, G.M. Pharr, J. Mater. Res. 11 (1996) 760.
[18] W. Herr, E. Broszeit, Surf. Coat. Technol. 97 (1997) 335.
[19] J. Musil, S. Kadlec, J. Vyskocil, V. Valvoda, Thin Solid Films 167 (1988) 107.
[20] V. Valvoda, R. Cerny, R. Kuzel, J. Musil, V. Poulek, Thin Solid Films 158 (1988) 225.
[21] G.M. Pharr, Mater. Sci. Eng. A253 (1998) 151.
[22] S.J. Bull, T.F. Page, E.H. Yoffe, Phil. Mag. Lett. 59 (1989) 281.
[23] C.A. Brookes, in: J.E. Field (Ed.), The Properties of Natural and Synthetic Diamond, Academic Press, San Diego, 1992, p. 521.
[24] S. Veprek, in: R. Riedel (Ed.), Handbook of Ceramic Hard Materials, 1, Wiley–VCH, Weinheim, 2000, p. 104.
[25] S. Veprek, A. Niederhofer, K. Moto, P. Nesladek, H. Männling, T. Bolom, Mater. Res. Soc. Symp. Proc. 581 (2000) 321.
[26] S. Timoshenko, J.N. Goodier, Theory of Elasticity, 2nd edition, McGraw Hill, New York, 1951.
[27] H.-H. Behnke, Härterei Zechnische Mitteilungen 48 (1993) 3.
[28] D.M. Teter, MRS Bulletin 23 (1) (1998) 22.
[29] M. Hebbache, Solid State Commun. 113 (2000) 427.
[30] T.Y. Tsui, G.M. Pharr, W.C. Oliver et al., Mater. Res. Soc. Symp. Proc. 383 (1995) 447.
[31] Ch. Kittel, Introduction to Solid State Physics, 4th edition, John Wiley, New York, 1971.
[32] A. Kelly, N.H. Macmillan, Strong Solids, Clarendon Press, Oxford, 1986.
[33] I.N. Sneddon, Int. J. Eng. Sci. 3 (1965) 47.
[34] A. Bolshakov, G.M. Pharr, Mater. Res. Soc. Symp. Proc. 436 (1997) 189.
[35] J.C. Hay, A. Bolshakov, G.M. Pharr, J. Mater. Res. 14n (1999) 2296.
[36] G. Tabor, The Hardness of Metals, Clarendon Press, Oxford, 1951.
[37] F.A. McClintock, A.S. Argon, Mechanical Behaviour of Materials, Addison–Wesley, Reading USA, 1966, chapter 13.
[38] G.M. Pharr, Mater. Res. Soc. Symp. Proc. 239n (1992) 301.
[39] I.V. Gridneva, Y.V. Milan, V.I. Trefilov, Phys. Status Solidi (a) 14 (1972) 177.
[40] R. Grover, I.C. Getting, G.C. Kennedy, Phys. Rev. B 7 (1973) 567.
[41] M.F. Rose, Phys. Status Solidi 17 (1966) K199.
[42] M.F. Rose, Phys. Status Solidi 21 (1967) 235.
[43] Landolt–Börnstein, Numerical Data and Functional Relationship in Science and Technology Group III: Crystal and Solid State Physics, Vol. 1, Springer–Verlag, Berlin 1966 p. 4.; ibid, Vol. 2, Springer–Verlag, Berlin 1969.
[44] M.H.G. Jacobs, H.A.J. Oonk, Phys. Chem. Chem. Phys. 2 (2000) 2641.
[45] J.H. Rose, J.R. Smith, F. Guinea, J. Ferrante, Phys. Rev. B 29 (1984) 29.
[46] J.R. Smith, J. Ferrante, P. Vinet, J.G. Gray, R. Richter, J.S. Rose, in: R.M. Latanisos, R.H. Jones (Eds.), Chemistry and Physics of Fracture, Martinus Nijhoff, Dordrecht, 1987, p. 329.
[47] W.C. Oliver, G.M. Pharr, J. Mater. Res. 7 (1992) 1564.